Wetting and dewetting of structured and imprinted surfaces[☆]

Reinhard Lipowsky *, Peter Lenz, Peter S. Swain

Max Planck Institut für Kolloid- und Grenzflächenforschung, Am Mühleuberg, 14476 Golm, Germany

Abstract

Wetting and dewetting of structured and imprinted surfaces is discussed from a theoretical point of view. An appropriate separation of length scales is used in order to eliminate irrelevant parameters from the theory. This leads to a general description of the wetting phase which can exhibit various morphologies such as droplets, channels or films. We discuss some general features of heterogeneous surfaces, extended surface domains, and line tension effects. We emphasize (i) the new concept of morphological wetting transitions, which occur both for small and for large surface domains; and (ii) the importance of studying the scale-dependence of the wetting morphologies as one zooms down into the nanoregime. © 2000 Elsevier Science B.V. All rights reserved.

Keywords: Wetting; Structured surfaces; Morphological transitions; Line tension

1. Introduction

Wetting and dewetting phenenoma are ubiquitous. The formation of rain droplets sitting on a plant leaf or hanging from a spider's web provide familiar examples of dewetting. On the other hand, the spreading of paint and adhesives on solid surfaces or the application of cosmetics onto the human skin rely on the wetting properties of these liquids. In fact, you could not read this article without the tear films which wet your eyes and which are stabilized by the closure of your eyelids.

The edge of a liquid droplet can be characterized by a certain contact angle θ, compare Fig. 1.

In the terminology used here, wetting and dewetting correspond to a lyophilic substrate surface with contact angle $0 \leq \theta < \pi/2$ and to a lyophobic surface with $\pi/2 < \theta < \pi$, respectively. For smooth and laterally uniform surfaces, such as those displayed in Fig. 1, the contact angle satisfies the classical Young equation which was first derived almost 200 years ago.

More recently, a lot of experimental effort has been devoted to the construction of laterally structured or imprinted surfaces with different types of surface domains. We will focus on the case with two types of domains which exhibit a relatively large wettability contrast for a given liquid. Thus, the liquid tends to wet the lyophilic domains but to dewet the lyophobic ones, i.e. it wants to maximize and to minimize the contact with the lyophilic and lyophobic surface regions,

---

[☆] In memory of Professor Hans-Jörg Jacobasch.

* Corresponding author.

respectively. As a result, the morphology of the wetting layer reflects the underlying pattern of surface domains.

The ambition of the experimentalist is to create relatively small surface patterns with domain sizes in the micrometer or even in the nanometer range. Using these patterns as two-dimensional templates, one may build up three-dimensional structures with a characteristic dimension which is comparable to the domain size. This should be useful for the manufacture of new micro- and nano-devices.

Wetting of structured or imprinted surfaces exhibits several unusual features which will be discussed here from a theoretical point of view [1–3]. First of all, droplet and channels on extended surface domains can exhibit contact angles which do not satisfy the classical Young equation. This property which is rather general and universal leads to new types of wetting transitions occurring between different wetting morphologies as will be discussed in the following sections.

Furthermore, as one creates smaller and smaller surface patterns on the micrometer or nanometer scale, one must ask if the corresponding wetting structures can be understood using the same theoretical framework as appropriate for the macroscopic scale, a question which is of fundamental interest to the science of colloids and interfaces. Indeed, sufficiently small structures should be governed by contributions from the contact lines but the sign and the magnitude of the associated line tensions are still rather controversial. We will argue below that a systematic study of wetting morphologies on structured surfaces will provide new information which should be useful in order to settle these controversies.

Several experimental methods are now available by which one can create surface patterns with domain sizes in the micrometer range. Three examples are: (i) elastomer stamps by which one can create patterns of hydrophobic alkanethiol on metal surfaces [4–6]; (ii) vapor deposition through grids which cover part of the surface [7]; and (iii) photolithography of amphiphilic monolayers which contain photosensitive molecular groups [8].

In addition, new experimental methods are being developed in order to construct patterns with even smaller domain sizes in the nanometer range. These methods include lithography with colloid monolayers [9], atomic beams modulated by light masks [10], and microphage separation in diblock copolymer films [11]. Thus, it will soon be possible to perform systematic wetting studies in which one varies the size of the underlying domain pattern over a wide range of length scales.

Our paper is organized as follows. First, the theoretical framework used to describe the wetting morphologies (droplets, channels, films) is presented in Section 2. We treat the general case of surfaces which are both topographically rough and chemically heterogeneous and obtain a generalized or modified Young equation for the local contact angle. This description is based on an appropriate separation of length scales as explained in Section 3. This latter section also contains a detailed discussion of the contact line tension. We then distinguish several types of heterogeneous surfaces and explain the concept of
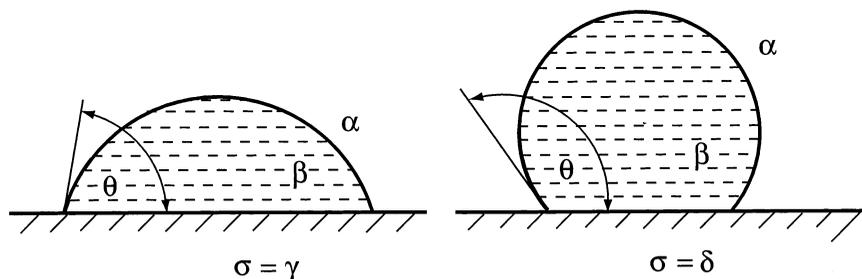
Fig. 1. (left) Wetting of a lyophilic substrate surface (γ) with contact angle $\theta < \pi/2$; (right) dewetting of a lyophobic surface (δ) with $\theta > \pi/2$.

extended surface domains in Section 4. Several examples of wetting morphologies on such surface domains are described in Section 5: liquid droplets on single domains and on lattices consisting of many domains, and liquid channels on striped surfaces. Finally, we extend our approach to line tension effects in Section 6 and give a brief outlook on related problems in Section 7.

Two appendices have been added. Appendix A describes the parametrization of the interfaces and contact lines, which is an important but somewhat technical aspect of our work. In addition, Appendix B contains a list of all the mathematical symbols used in this paper.

Even though this paper is basically a review, it also contains several new aspects: (i) an analytical calculation of the line tension, see Section 3.3; (ii) interfacial folds emanating from the contact line, see Section 4.2; (iii) vesicles adhering to a structured or imprinted surface, see Section 5.1; and (iv) kinks in the shape of the contact line, see Section 6.

For the sake of clarity, we always use the terminology as appropriate to liquid–vapor systems. However, our theoretical framework applies to all systems which are at or close to two-phase coexistence [12] and which are in contact with a structured or imprinted surface. Two rather different examples are: (i) a binary (or ternary) liquid mixture at (or close to) two-phase coexistence and adjacent to a structured or imprinted container wall; and (ii) a solid close to its melting point and in contact with a structured surface. In the latter case, the solid would start to melt from well-defined surface domains (in general, one should include the anisotropy of the solid–melt interface and possible elastic strains within the solid).

2. Theoretical description

2.1. Morphologies of the wetting phase

Consider a solid substrate, denoted by (σ), which is rigid and inert in the presence of a vapor phase (α). The substrate surface is, on average, parallel to a reference plane with coordinates $\mathbf{x} \equiv (x_1, x_2)$; the coordinate perpendicular to this plane will be denoted by z.

Now, let us place a certain amount of wetting phase (β) on the substrate surface. What we would like to determine is the shape or the morphology assumed by this (β) phase. More precisely, we are primarily interested in equilibrium states, i.e. in morphologies which are at least locally stable with respect to small perturbations of the shape.

Depending on the underlying substrate, the (β) phase may form a variety of different wetting structures: a single droplet, a pattern of disconnected droplets, a perforated or continuous wetting layer, or even bridges between disconnected domains within the substrate surface. These morphologies are primarily distinguished by the shape of the interfaces bounding the (β) phase.

The $(\beta\sigma)$ interfaces lie within the substrate surface. As mentioned, the substrate is taken to be rigid and inert and, thus, can be treated as a non-deformable wall. The $(\alpha\beta)$ interfaces on the other hand, adapt their shape to the constraints arising from the overall amount of (β) phase and from heterogeneities present within the substrate surface. Thus, the morphologies of the wetting phase are distinguished by the different shapes of the $(\alpha\beta)$ interfaces. These interfaces intersect the substrate surface along contact lines which represent their boundaries of the $(\alpha\beta)$ interfaces.

A detailed theoretical description of such a system could start with the molecules contained in the (α) and (β) phases. Thus, let us assume that these phases contain several species of molecules, labelled by $j = 1, 2, \ldots$ In equilibrium, the system is then described by densities $N_j = N_j(\mathbf{x}, z)$ which represent the particle number of species j per unit volume. In order to distinguish the two phases α and β, we typically need to consider only one of these densities, say $N_1(\mathbf{x}, z)$.

Away from the $(\alpha\beta)$ interfaces, the density $N_1(\mathbf{x}, z)$ has the values N_α and N_β in the (α) and (β) phases, respectively. In the interfacial region, this density interpolates smoothly between N_α and N_β. [13] Thus, we may define the position of the $(\alpha\beta)$ interfaces by the implicit equation $N_1(\mathbf{x}, z) = N_{\alpha\beta}$ for some $N_{\alpha\beta}$ satisfying $N_\alpha < N_{\alpha\beta} < N_\beta$. It is far more convenient, however, to use a theoretical description which focuses directly on the interfacial shape. This is the approach used here.

Therefore, we will concentrate on the interfacial shape and use a theoretical description which starts from a general parametrization of this shape, see Appendix A.1. In addition to the free energies associated with these interfaces, we will also include additional contributions arising from the contact lines. For flat substrate surfaces, these contact lines are planar curves which simplifies their parametrization, see Appendix A.2.

2.2. Free energy of the wetting phase

For any piece of matter, thermodynamics gives three different contributions to its free energy: the first contribution is proportional to the volume of the material, the second to its surface area, and the third to the length of its edges. It is straightforward to apply this general framework to the wetting structures studied here. These structures occupy a spatial region $\mathcal{V}_\beta$ of (β) phase which has volume $V_\beta \equiv |\mathcal{V}_\beta|$ and which is bounded by interfaces $\mathcal{A}_{\alpha\beta}$ and $\mathcal{A}_{\beta\sigma}$ with surface areas $A_{\alpha\beta} \equiv |\mathcal{A}_{\alpha\beta}|$ and $A_{\beta\sigma} \equiv |\mathcal{A}_{\beta\sigma}|$, respectively. These two interfaces intersect along the contact lines denoted by $\mathcal{L}_{\alpha\beta\sigma}$, which have a total length $L_{\alpha\beta\sigma} \equiv |\mathcal{L}_{\alpha\beta\sigma}|$.

The total free energy functional of the wetting phase is then given by

$$\mathcal{F} = (V_\beta - V_o)\Delta P + \mathcal{F}_\Sigma + \mathcal{F}_\Lambda \qquad (2.1)$$

The first term depends on the difference $\Delta P \equiv P_\alpha - P_\beta$ between the pressures in the (α) and (β) phases. In the fixed volume ensemble with $V_\beta \equiv V_o$, as considered in Section 5 below, the parameter ΔP is a Lagrange multiplier and this term does not contribute to the free energy.

For sufficiently large layers and droplets, gravity leads to an additional term. If the fluid phases (α) and (β) contain several species of particles labelled by j with particle mass m_j and mean densities $N_{\beta j}$, $N_{\alpha j}$, the gravitational term is given by the volume integral of $\Sigma_j(N_{\beta j} - N_{\alpha j})m_j g z$ where g and z are the gravitational acceleration and the coordinate perpendicular to the substrate, respectively. We need not discuss these terms since we will focus on wetting structures in the submillimeter range, for which the effects of gravity are small and can be ignored.

The second free energy term $\mathcal{F}_\Sigma$ in Eq. (2.1) contains the contributions which arise from the interfacial tensions Σ and is given by

$$\mathcal{F}_\Sigma = \int dA_{\alpha\beta}\Sigma_{\alpha\beta} + \int dA_{\beta\sigma}[\Sigma_{\alpha\beta} - \Sigma_{\alpha\sigma}] \qquad (2.2)$$

which measures the excess free energy of the interfaces arising from the (β) phase. The interfacial tension $\Sigma_{\alpha\beta}$ of the fluid–fluid interface is taken to be uniform as appropriate for a laterally homogeneous interface. In contrast, the substrate surface may contain chemical heterogeneities which lead to position-dependent tensions $\Sigma_{\beta\sigma} = \Sigma_{\beta\sigma}(\mathbf{x})$ and $\Sigma_{\alpha\sigma} = \Sigma_{\alpha\sigma}(\mathbf{x})$ where $\mathbf{x} \equiv (x_1, x_2)$ represents the surface coordinate of the (σ) substrate as already mentioned.

The third free energy term $\mathcal{F}_\Lambda$ in Eq. (2.1) arises from the contact lines and depends on the corresponding line tension $\Lambda = \Lambda(\mathbf{x})$. This free energy term has the form

$$\mathcal{F}_\Lambda = \int d\mathcal{L}_{\alpha\beta\sigma}\Lambda \qquad (2.3)$$

In general, the line tension Λ can be positive or negative [13] and thus the free energy contribution $\mathcal{F}_\Lambda$ can have either sign as well. It has recently been claimed that the line tension is positive for wetting of solid substrates [14] but the arguments used in order to arrive at this conclusion are not convincing.

The equilibrium shape of the droplets is determined by minimization of the free energy as discussed in the next subsection. In addition, one may also expand the free energy functional around these shapes and so study their stability. Such a stability analysis has been performed for the first two terms in Eq. (2.1), i.e. for $\Lambda = 0$ as described elsewhere. [15,16]

2.3. Equilibrium shape of droplets

In order to minimize the free energy as given by Eq. (2.1), one considers an (α, β) interface of arbitrary shape and performs small displacements of this interface. Interfacial shapes of minimal free energy are found from the requirement that all variations of the free energy, which are of first order in the displacements, must vanish. From the

first two terms in Eq. (2.1), one then obtains the well-known Laplace equation

$$2M\Sigma_{\alpha\beta} = P_\beta - P_\alpha \qquad (2.4)$$

for the mean curvature M of the (α, β) interface. Since both $\Sigma_{\alpha\beta}$ and $P_\beta - P_\alpha$ are constant, the $(\alpha\beta)$ interface is characterized by constant mean curvature. As explained in Appendix A, we define the mean curvature M in such a way that it is positive for a spherical surface.

In the derivation of the Laplace equation (2.4), it is sufficient to consider surface displacements along the surface normals (denoted by $\hat{N}$ in Appendix A.1). However, at the boundary of the $(\alpha\beta)$ interface, i.e. at the contact line, the variational calculation is more subtle: one has to consider both normal and tangential surface displacements in order to ensure that the contact line stays within the substrate surface. Such a calculation has been done for zero line tension, i.e. in the absence of the free energy term (2.3). [1]

Alternatively, the minimization of the free energy may be performed in two steps. First, one determines the shapes of minimal free energy for a particular configuration of the contact line. Secondly, the resulting free energy is minimized with respect to the location of this line. The latter calculation has been performed for the general case defined by the free energies (2.1)–(2.3) with line tension $\Lambda = \Lambda(\mathbf{x})$. [2] As a result, one arrives at the generalized or modified Young equation

$$\Sigma_{\alpha\beta}\cos(\theta(\mathbf{x})) = \Sigma_{\alpha\sigma}(\mathbf{x}) - \Sigma_{\beta\sigma}(\mathbf{x}) - \Lambda(\mathbf{x})C_{\alpha\beta\sigma}$$
$$- (\nabla_x\Lambda(\mathbf{x})) \cdot \hat{n} \qquad (2.5)$$

The variable $C_{\alpha\beta\sigma}$ and the unit vector $\hat{n}$ represent the geodesic curvature and a certain normal vector to the contact line, respectively, see Appendix A.2. The symbol ∇_x is the two-dimensional gradient with respect to the coordinate $\mathbf{x}$ of the substrate surface.

For contact lines which lie within a planar substrate as considered below, the two line tension terms in Eq. (2.5) can be combined which leads to

$$\Sigma_{\alpha\beta}\cos(\theta(\mathbf{x})) = \Sigma_{\alpha\sigma}(\mathbf{x}) - \Sigma_{\beta\sigma}(\mathbf{x}) - \nabla_x \cdot (\Lambda(\mathbf{x})\hat{n})$$
$$\qquad (2.6)$$

If line tension terms can be ignored, the modified Young equation has the same functional form as the usual Young equation but the interfacial tensions $\Sigma_{\alpha\sigma}$ and $\Sigma_{\beta\sigma}$ depend on the surface coordinate $\mathbf{x}$. [1] Special cases of the line tension terms have been previously derived for planar and homogeneous surfaces [17], for surface heterogeneities which are axially symmetric [18] and for heterogeneities which are translationally invariant with respect to one surface coordinate [19]. As far as we know, the general form of the line tension term as given by Eq. (2.5) was first derived in [2].

3. Separation of length scales

The theoretical framework described in the previous section is useful since it depends only on a relatively small number of parameters. It is important to realize, however, that it involves several implicit assumptions. These assumptions will now be discussed.

First, we have ignored the effects of gravity which is convenient in order to eliminate some parameters from the description. It is rather straightforward, however, to include these effects in our theoretical framework. The main effect of gravity is that the wetting structures assume a certain maximal thickness as soon as L_β becomes comparable to the capillary length L_{cap}. This latter length scale is usually in the millimeter range.

Secondly, the size L_β of the wetting structure is taken to be large compared to the size ℓ_{mol} of the molecules. Similarly, we will also assume that L_β is large compared to those microscopic length scales which are related to the small-scale structure of the different interfaces. It turns out that there are several such scales which will be discussed in the following.

3.1. Properties of the ($\alpha\beta$) interface

The first quantity to be discussed is the intrinsic width, $\ell_{\alpha\beta}$, of the $(\alpha\beta)$ interfaces between the two fluid phases. Thus, imagine taking snapshots of these interfaces (with an exposure time of the order of picoseconds). The intrinsic width represents the local fuzziness which an interface would

exhibit in these snapshots, i.e. the thin spatial region in which the densities differ significantly from their values in the two adjacent phases.

These two phases, (α) and (β), are taken to be at or close to $(\alpha\beta)$ coexistence but away from any critical point. Thus, the correlation length, ξ_β within the wetting phase (β) is of the order of the molecular size ℓ_{mol}. Since the intrinsic width $\ell_{\alpha\beta}$ is proportional to ξ_β, this width is also of the order of ℓ_{mol}.

Next, let us estimate the interfacial tension $\Sigma_{\alpha\beta}$ by a simple but useful scaling argument. In the liquid state, the free energy per unit volume is of the order of T/ℓ_{mol}^3, where ℓ_{mol} is the molecular size as before. The interfacial tension of the $(\alpha\beta)$ interface can now be estimated by integrating this free energy density over the interfacial width $\ell_{\alpha\beta}$ which leads to

$$\Sigma_{\alpha\beta} \simeq (T/\ell_{mol}^3)\ell_{\alpha\beta} \simeq (\ell_{\alpha\beta}/\ell_{mol}) \times 50 \ \ \text{mJ} \ \ \text{m}^{-2} \tag{3.1}$$

where the last estimate holds for room temperature $T = 4 \times 10^{-21}$ J and $\ell_{mol} = 0.3$ nm. The experimental values for the interfacial tension lie in the range of 10–10^2 mJ m^{-2} which implies that $\ell_{\alpha\beta} \simeq \ell_{mol}$.

In principle, the interfacial width is also affected by thermally excited shape fluctuations. As a result of these fluctuations, the interfaces acquire a certain roughness which is proportional to $(T/\Sigma_{\alpha\beta})^{1/2}\sqrt{\ln(L_\beta/\ell_{mol})}$. From the estimate of the interfacial tension $\Sigma_{\alpha\beta}$ as given by Eq. (3.1), one concludes that the prefactor $(T/\Sigma_{\alpha\beta})^{1/2}$ is again of the order of the molecular size ℓ_{mol}. Therefore, the interfacial roughness is comparable to the intrinsic width, and its presence does not change the above estimates in any significant way.

3.2. Simple view of the contact line

The contact lines represent the edges or boundaries of the $(\alpha\beta)$ interfaces along the substrate surface. The structure of such a line depends both on the $(\alpha\beta)$ interface and on the substrate surface. If this surface is flat and laterally homogeneous, the contact line structure is primarily determined by the intermolecular forces between the substrate and the molecules within the fluid phases as considered in the next subsection. If the substrate is topographically rough and/or chemically heterogeneous, these features will also affect the contact line.

In the present subsection, we will assume that the cross-section of the contact line is more or less isotropic and can be characterized by a certain width, $\ell_{\alpha\beta\sigma}$. This width may vary along the substrate surface as one would expect, in general, for a heterogeneous surface. The length scale $\ell_{\alpha\beta\sigma}$ will now be used in order to estimate the magnitude of the line tension Λ.

As mentioned previously, the free energy density within the fluid phases is of the order of T/ℓ_{mol}^3. To estimate the line tension Λ, one has to integrate this free energy density over the intrinsic area $\simeq \ell_{\alpha\beta\sigma}^2$ of the contact line cross section. In this way, one obtains

$$|\Lambda| \simeq (T/\ell_{mol}^3)\ell_{\alpha\beta\sigma}^2 \simeq \Sigma_{\alpha\beta}\ell_{\alpha\beta\sigma}^2/\ell_{\alpha\beta}$$
$$\simeq (\ell_{\alpha\beta\sigma}/\ell_{mol})^2 \times 10^{-11} \ \ \text{J} \ \ \text{m}^{-1} \tag{3.2}$$

where the last estimate applies to room temperature $T = 4 \times 10^{-21}$ J and $\ell_{mol} = 0.3$ nm.

The numerical values for the line tension $|\Lambda|$, which have been deduced experimentally, vary over a wide range as given by 10^{-11} J m$^{-1} \lesssim |\Lambda| \lesssim 10^{-6}$ J m^{-1} [20,14,21,22]. It is instructive to use (3.2) in order to express $|\Lambda|$ in terms of the length scale $\ell_{\alpha\beta\sigma}$. The range of $|\Lambda|$ values then corresponds to $1 \lesssim \ell_{\alpha\beta\sigma}/\ell_{mol} \lesssim 300$.

Note that we avoided interpreting the contact line width $\ell_{\alpha\beta\sigma}$ in a specific way. Thus, this width could represent an intrinsic width which one would observe as a local variation of the densities close to the contact line. Such an intrinsic width will be calculated in the next subsection. Alternatively, the width $\ell_{\alpha\beta\sigma}$ could also contain contributions from a certain roughness of the contact line. One example for contact line roughening is discussed below in Section 4.3. In this latter case, we would consider the line tension as estimated by Eq. (3.2) to represent a coarse-grained or effective quantity. Those values of $|\Lambda|$ which are large compared to 10^{-9} J m^{-1} — corresponding to contact line widths $\ell_{\alpha\beta\sigma}$ which are large compared to $10 \ \ell_{mol}$ — are likely to represent such effective line tensions.

3.3. More detailed view of the contact line

A more detailed description of the contact line can be obtained in the framework of effective interface models. In general, the molecules within the substrate and the fluid phases interact via various intermolecular forces such as, e.g. van der Waals and electrostatic interactions. For a thin wetting layer of thickness l, these intermolecular forces lead to an effective interface potential, $U(l)$, which represents the layer free energy per unit area.

In this subsection, we will consider flat and laterally homogeneous substrate surfaces. More precisely, we will assume that the length scales which characterize the geometric roughness and the chemical heterogeneities of such a surface are of the order of the molecular size ℓ_{mol}. The interface potential $U(l)$ can be calculated by a variety of methods [12]. For short-ranged forces between the atoms or molecules, one obtains interface potentials which decay exponentially with the wetting layer thickness as can be derived from local functionals of the particle number densities [23,24]. For long-ranged forces such as van der Waals interactions, these potentials decay as inverse power laws, see e.g. [25–27].

For incomplete wetting at $(\alpha\beta)$ coexistence, the potential $U(l)$ exhibits a minimum at the finite layer thickness $l = l_{\mathrm{min}}$ and approaches a constant value for large values of l. More precisely, one has

$$U(l) \approx \Sigma_{\alpha\beta} + \Sigma_{\beta\sigma} \quad \text{for large } l \tag{3.3}$$

and

$$U(l) \approx \Sigma_{\alpha\sigma} + \frac{1}{2}(\Sigma_{\alpha\beta}/\xi_{\alpha\beta}^2)(l - l_{\mathrm{min}})^2 \tag{3.4}$$

for l values close to $l = l_{\mathrm{min}}$. The length scale $\xi_{\alpha\beta}$ is the interfacial correlation length which governs the $\mathbf{x}$-variation of the thickness in response to a local perturbation; away from this perturbation, the average thickness profile exhibits the exponential decay $\langle l(\mathbf{x}) \rangle \sim \exp(-|\mathbf{x}|/\xi_{\alpha\beta})$.

In the simplest case, the interface potential has no barrier between the minimum at $l = l_{\mathrm{min}}$ and its constant value at large l. In this case, the interface potential has only one point of inflection at $l = l_{\mathrm{pin}}$. A rough estimate for l_{pin} is obtained from

$$l_{\mathrm{pin}} \simeq l_* \equiv l_{\mathrm{min}} + \sqrt{2(1 - \cos(\theta_\infty))}\,\xi_{\alpha\beta} \tag{3.5}$$

where l_* represents that value of l, at which the two asymptotic forms of $U(l)$, as given by the Eqs. (3.3) and (3.4), intersect.

In Eq. (3.5), we have introduced the asymptotic value θ_∞ of the contact angle which satisfies the classical Young equation, i.e. $\Sigma_{\alpha\beta}\cos(\theta_\infty) \equiv \Sigma_{\alpha\sigma} - \Sigma_{\beta\sigma}$. The latter relation is obtained from the generalized Young equations (2.5) and (2.6) in the limit of large droplets or small contact line curvatures on a laterally homogeneous substrate as considered in this subsection. In this way, we ensure that the more microscopic model used here is consistent with our general theoretical framework as discussed in Section 2.

For contact angles θ small compared to $\pi/2$, one may use the Monge parametrization $l = l(\mathbf{x})$ for the droplet shape. To leading order in the gradients of l, the corresponding free energy is given by

$$\mathscr{F}\{l\} \approx \int d\mathbf{x}\left[\frac{1}{2}\Sigma_{\alpha\beta}(\nabla_x l)^2 + U(l) + \Delta P l\right] \tag{3.6}$$

where $\Delta P = P_\alpha - P_\beta \leq 0$ again plays the role of a Lagrange multiplier for the total volume of the droplet or, more precisely, for the excess volume of the droplet with interface position $l > l_{\mathrm{min}}$.

The shape of the droplet can now be calculated by minimization of the functional $\mathscr{F}\{l\}$ as given by Eq. (3.6). One then obtains droplets which are surrounded by a thin layer of (β) phase with thickness $l = l_{\mathrm{min}}$. This layer lies within the $(\alpha\sigma)$ interface and tends to increase the intrinsic width of this interface.

In the theoretical framework just described, the contact line corresponds to the spatial region between (i) the thin layer of thickness $l = l_{\mathrm{min}}$ and (ii) the region occupied by the droplet. The average thickness profile $\langle l \rangle = \langle l(\mathbf{x}) \rangle$ obtained by minimization of the free energy functional (3.6) can be easily calculated if one approximates the interface potential $U(l)$ by its asymptotic forms as given by Eqs. (3.3) and (3.4). One then finds that the lateral extension of the spatial region corresponding to the contact line is governed by the correlation length $\xi_{\alpha\beta}$ as introduced in Eq. (3.4). Likewise, the scale for the perpendicular extension

of this region is set by the thickness l_{pin} where $U(l)$ has its point of inflection.

Within the calculation just described, the line tension Λ is obtained by inserting the average thickness profile into the functional $\mathcal{F}$ as given by Eq. (3.6), i.e. from $\mathcal{F}\{\langle l(\mathbf{x})\rangle\}$. Using again the asymptotic forms of $U(l)$, one obtains

$$\Lambda = (\Sigma_{\alpha\beta} + \Sigma_{\beta\sigma} - \Sigma_{\alpha\sigma})\xi_{\alpha\beta} = (1 - \cos(\theta_\infty))\Sigma_{\alpha\beta}\xi_{\alpha\beta} \tag{3.7}$$

In the first equality, the line tension Λ is expressed in terms of the model parameters, i.e. in terms of the three interfacial tensions and the interfacial correlation length $\xi_{\alpha\beta}$. In the second equality, we have again inserted the relation $\Sigma_{\alpha\beta}\cos(\theta_\infty) = \Sigma_{\alpha\sigma} - \Sigma_{\beta\sigma}$ for the asymptotic value θ_∞ of the contact angle as introduced in Eq. (3.5). As a result, the line tension is now expressed in terms of three measurable quantities. Comparison with the dimensional estimate (3.2) shows that, within the more microscopic model used here, the length scale $\ell_{\alpha\beta\sigma}^2/\ell_{\alpha\beta}$ corresponds to $(1 - \cos(\theta_\infty))\xi_{\alpha\beta}$.

3.4. Interfacial versus line tensions

It is intuitively clear that the effects of line tension can be ignored for sufficiently large wetting structures. We will now use the previous estimates for the different tensions in order to determine the corresponding regimes. Thus, consider a (β) droplet (or another wetting structure) of linear dimension L_β which is large compared to the contact line width $\ell_{\alpha\beta\sigma}$.

The interfacial contribution to its free energy, $\mathcal{F}_\Sigma$, is of the order of

$$\mathcal{F}_\Sigma \simeq L_\beta^2 \Sigma_{\alpha\beta} \simeq (L_\beta^2 \ell_{\alpha\beta}/\ell_{\text{mol}}^3)T \tag{3.8}$$

where the estimate (3.1) has been used. Likewise, we find from (3.2) that the contact line contribution to the free energy is of the order of

$$|\mathcal{F}_\Lambda| \simeq L_\beta|\Lambda| \simeq (L_\beta \ell_{\alpha\beta\sigma}^2/\ell_{\text{mol}}^3)T \tag{3.9}$$

Using these estimates, the ratio of the two free energy contributions is found to be

$$|\mathcal{F}_\Lambda|/\mathcal{F}_\Sigma \simeq (\ell_{\alpha\beta\sigma}^2/L_\beta\ell_{\alpha\beta}) \tag{3.10}$$

This ratio becomes of order one and both free energy contributions are equally important if the wetting structure has the linear dimension $L_\beta = L_\beta^*$ with

$$L_\beta^* \simeq |\Lambda|/\Sigma_{\alpha\beta} \simeq \ell_{\alpha\beta\sigma}^2/\ell_{\alpha\beta} \tag{3.11}$$

As a numerical example, consider the values $\ell_{\alpha\beta}^\sigma \simeq 10 \ \ell_{\text{mol}}$ and $\ell_{\alpha\beta} \simeq \ell_{\text{mol}} \simeq 0.3$ nm. If these values are inserted into (3.10), one obtains

$$|\mathcal{F}_\Lambda|/\mathcal{F}_\Sigma \simeq 10^2(\ell_{\text{mol}}/L_\beta) \tag{3.12}$$

which leads to $|\mathcal{F}_\Lambda|/\mathcal{F}_\Sigma \simeq 1$, 10^{-1}, and 10^{-3} for $L_\beta = 30$ nm, 300 nm and 30 μm, respectively.

Thus, for line tensions $|\Lambda|$ of the order of 10^{-9} J m^{-1} corresponding to line widths $\ell_{\alpha\beta\sigma}$ of the order of 3 nm, the contact line contributions to the free energy are of the same order as the interfacial contributions if the linear dimension L_β of the wetting structures is $\simeq 30$ nm. In this case, the morphology of the wetting phase is determined both by the interfacial and by the line tensions.

For somewhat larger structures with $L_\beta \simeq 300$ nm, the line tension contribution should represent a correction term but its presence should still have a noticable effect on the wetting morphology. For relatively large wetting structures, on the other hand, which have a characteristic dimension of the order of many micrometers, the free energy contributions arising from the line tension are much smaller than the interfacial free energies, and the line tension should not affect the shape of the wetting phase in any significant way.

In Section 5 below, we will consider such relatively large wetting structures with $L_\beta \gg L_\beta^* \simeq |\Lambda|/\Sigma_{\alpha\beta}$. For the case of wetting channels on striped surface domains as discussed in Section 5.3, we have made a detailed comparison between the theoretical and the experimental wetting morphologies. This comparison clearly shows that the line tension has no significant effect on the micrometer scale and that its value must lie below 10^{-7} J m^{-1}. Finally, in Section 6, we will briefly look at wetting morphologies on scales below L_β^* and discuss some effects arising from line tension terms.

4. Heterogeneous substrate surfaces

In general, the substrate surface may be topographically rough and/or chemically heterogeneous. As before, the substrate surface is taken to be rigid and inert. Thus, the shape of this surface represents a 'quenched' or 'frozen' quantity which does not change on relevant time scales. This shape will typically deviate from a plane and will exhibit transverse excursions. The corresponding roughness of the substrate surface will be denoted by $\ell_{\sigma\perp}$. Here and below, we will assume that $\ell_{\sigma\perp}$ is too small to influence the wetting structures in a significant way. Thus, the surface is assumed to be essentially flat on the relevant length scales.

As far as the chemical heterogeneities are concerned, several cases are accessible to experiment and will be distinguished: (i) small-scale heterogeneities on a microscopic scale $\ell_{\sigma\|}$ which is of the order of a few molecular sizes and, thus, is much smaller than the linear dimension L_β of the wetting structure; (ii) smooth composition variations on length scales $L_{\sigma\|}$ which are large compared to $(\ell_{\sigma\|}$ but still small compared to L_β; and (iii) extended surface domains corresponding to structured or imprinted surfaces. These surface domains, which will be denoted by (γ) and (δ), have a uniform composition and a typical size L_γ and L_δ, respectively. In this latter case, one obtains morphological transitions if the linear dimension L_β of the wetting structures becomes comparable to the domain sizes.

4.1. Position-dependent surface composition

For a substrate surface composed of several atomic (or molecular) species, we will first coarse grain up to a certain length scale $\ell_{\sigma\|}$, which is somewhat larger than the molecular scales, in order to define appropriate composition variables. In the simplest case of a binary system, we need only one such composition variable which may be defined, e.g. as the relative area fraction of one of the two species in the surface layer. In this way, we arrive at coarse grained composition variables, say ϕ. In general, these composition variables will still vary along the substrate surface, i.e. $\phi = \phi(\mathbf{x})$, corresponding to composition gradients present on larger scales.

For a chemically homogeneous surface characterized by uniform, i.e. position-independent composition variables $\phi = \phi_0$, one may define the excess free energies or interfacial tensions $\Sigma_{\alpha\sigma}$ and $\Sigma_{\beta\sigma}$ in the usual way. [13] The values of these tensions will of course, depend on the values of the composition variables: $\Sigma_{\alpha\sigma} = \Sigma_{\alpha\sigma}(\phi_0)$ and $\Sigma_{\beta\sigma} = \Sigma_{\beta\sigma}(\phi_0)$. Thus, in the heterogeneous case with $\phi = \phi(\mathbf{x})$, one may allude to a small gradient expansion and assume that the local tensions are given by $\Sigma = \Sigma(\phi(\mathbf{x}))$, i.e. they are essentially determined by the local surface composition.

In principle, one may attempt to use a more detailed description for the intermolecular forces between the heterogeneous substrate and the molecules within the fluid phases. For example, various approximation schemes have been used in order to include the van der Waals forces arising from a substrate surface with two (or a few) surface domains. [28–30] We will not use such an approach here because it involves additional parameters which complicate the theoretical treatment but are irrelevant as long as the length scales introduced by the intermolecular forces are small compared to the overall size L_β of the wetting structure.

4.2. Cassie equation and effective contact angles

In some cases, the surface composition variables ϕ attain uniform values as soon as one considers length scales above a certain characteristic length $L_{\sigma\|}$. If we place a relatively large droplet with linear dimension $L_\beta \gg L_{\sigma\|}$ on such a substrate surface, this droplet will then see mean surface compositions and mean interfacial tensions as obtained by a spatial average over the surface coordinate $\mathbf{x}$. If the surface contains two components, for example, this spatial average leads to

$$\overline{\Sigma_{\alpha\sigma}(\mathbf{x}) - \Sigma_{\beta\sigma}(\mathbf{x})} = \phi_1(\Sigma_{\alpha1} - \Sigma_{\beta1}) + \phi_2(\Sigma_{\alpha2} - \Sigma_{\beta2})$$

(4.1)

where ϕ_i is the area fraction of surface component i. When this average is inserted into the generalized Young equation (2.5) (without the line tension terms), one obtains [2]

$$\Sigma_{\alpha\beta} \cos(\theta_{\text{eff}}) \equiv \phi_1(\Sigma_{\alpha1} - \Sigma_{\beta1}) + \phi_2(\Sigma_{\alpha2} - \Sigma_{\beta2})$$

(4.2)

which defines the effective contact angle θ_{eff}. This latter relation represents the so-called Cassie equation [31].

4.3. Interfacial folds emanating from the contact line

In order to get a more detailed picture of the droplet morphology, let us assume (i) that the surface compositions exhibit some oscillatory variations on the length scale $L_{\sigma\|}$, and (ii) that the intrinsic width of the contact line is small compared to $L_{\sigma\|}$. The contact line will then exhibit 'frozen' undulations with a characteristic wave length $\simeq L_{\sigma\|}$. Such undulations lead to folds along the $(\alpha\beta)$ interface which emanate from the contact line and which have a linear extension of the order of $L_{\sigma\|}$ as shown in the next paragraph. Therefore, one has to coarse-grain up to the length scale $L_{\sigma\|}$ in order to observe the effective contact angle θ_{eff} which satisfies the Cassie equation (4.2).

As a simple example, consider a contact line which is deformed according to $x_2(x_1) \sim \sin(\pi x_1 / L_{\sigma\|})$ within the flat substrate surface. A general deformation of the contact line may be described by a superposition of such Fourier modes. For simplicity, the contact angle of the $(\alpha\beta)$ interface, which extends into the half space with perpendicular coordinate $z > 0$, is taken to be close to $\theta = \pi/2$. The shape of this interface is then given by

$$h(x_1, z) \sim \sin(\pi x_1 / L_{\sigma\|}) \exp(-\pi z / L_{\sigma\|}) \qquad (4.3)$$

which satisfies the boundary condition $h(x_1, 0) \sim x_2(x_1) \sim \sin(\pi x_1 / L_{\sigma\|})$ and corresponds to a minimal surface with zero mean curvature (to leading order in the gradients of h). The functional dependence as given by Eq. (4.3) shows explicitly that a contact line, which exhibits 'frozen' undulations with wavelength $L_{\sigma\|}$ along the substrate surface, leads to folds which affect the interface up to a distance $z \simeq L_{\sigma\|}$ from the contact line.

4.4. Extended surface domains

Finally, we turn to the case of structured or imprinted surfaces. As explained in the introduc-

tion, several experimental methods are available by which one can create these surfaces with domain sizes in the micrometer range. As a result of these procedures, the substrate surface contains different types of domains with different wetting properties.

We will focus on patterns with two different surface domains: lyophilic domains denoted by (γ) and lyophobic domains denoted by (δ). The (γ) and the (δ) domains are homogeneous on scales large compared to $L_{\sigma\|}$ and have a lateral extension L_{γ} and L_{δ}, respectively, which are both much greater than $L_{\sigma\|}$. In principle, the width $L_{\gamma\delta}$ of the $(\gamma\delta)$ domain boundaries could be comparable in size to $L_{\sigma\|}$ but, in practice, the domain boundary width $L_{\gamma\delta}$ is determined by the experimental procedures, used to construct the structured or imprinted surface, and will typically exceed $L_{\sigma\|}$. In any case, we will focus on the case where the domain sizes are much larger than the domain boundary width, i.e. on situations with $L_{\gamma\delta} \ll L_{\gamma}$ and $L_{\gamma\delta} \ll L_{\delta}$.

The latter limit is convenient since the interfacial free energies of the substrate surface become piece-wise constant functions, and the position-dependent tension $\Sigma_{\beta\sigma}$ of the substrate surface is simply given by [1]

$$\Sigma_{\beta\sigma}(\mathbf{x}) = \Sigma_{\beta\gamma} \text{ for } \mathbf{x} \text{ in the } (\gamma) \text{ domains}$$

$$= \Sigma_{\beta\delta} \text{ for } \mathbf{x} \text{ in the } (\delta) \text{ domains} \qquad (4.4)$$

Likewise, one has $\Sigma_{\alpha\sigma}(\mathbf{x}) = \Sigma_{\alpha\gamma}$ and $\Sigma_{\alpha\delta}$ for $\mathbf{x}$ in the (γ) and (δ) domains, respectively.

Since the interfacial tensions are taken to be constant within the surface domains, a droplet which is located completely within a (γ) or within a (δ) domain forms a spherical cap with contact angle θ_{γ} or θ_{δ}, respectively. These latter angles satisfy the Young relations

$$\Sigma_{\alpha\beta} \cos(\theta_{\gamma}) = \Sigma_{\alpha\gamma} - \Sigma_{\beta\gamma} \text{ and}$$

$$\Sigma_{\alpha\beta} \cos(\theta_{\delta}) = \Sigma_{\alpha\delta} - \Sigma_{\beta\delta} \qquad (4.5)$$

as appropriate for each type of surface domain.

It turns out, however, that the droplets can also exhibit contact angles θ which are different both from θ_{γ} and from θ_{δ}. This happens as soon as the position of the contact line coincides with the position of the $(\gamma\delta)$ domain boundary.
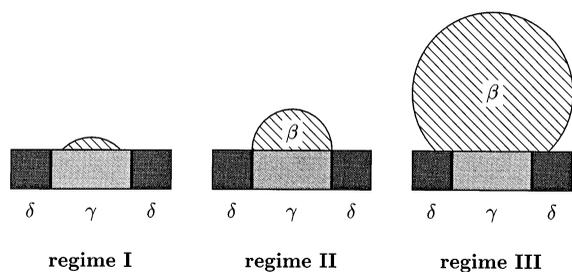
Fig. 2. Droplet on single lyophilic domain in a lyophobic matrix — depending on the droplet volume, the droplet state belongs to regime I with contact angle $\theta = \theta_\gamma$, to regime III with $\theta = \theta_\delta$, or to regime II in which the contact angle can freely adopt any value within the range $\theta_\gamma < \theta < \theta_\delta$.

5. Droplets, channels and films

5.1. Droplet on a single surface domain

As a simple example, consider a single lyophilic (γ) domain, which has a circular shape, embedded in a lyophobic (δ) matrix. If we place a small amount of liquid onto this domain, it forms a spherical cap with contact angle θ_γ. As we add more liquid to this droplet, it grows until it covers the whole (γ) domain. At this point, the contact line sits on top of the surface domain boundary ($\gamma\delta$). If we continue to add liquid, the contact area of the droplet remains fixed while the contact angle grows until it reaches the value θ_δ. Beyond this point, the droplet starts to increase its contact area and to spread onto the lyophobic matrix where it attains the contact angle θ_δ.

Thus, one must distinguish three different droplet regimes (I)–(III), as indicated in Fig. 2. Regime (I) corresponds to sufficiently small droplets which are located within the (γ) domain and have contact angle θ_γ. Regime (III) is given by sufficiently large droplets which have spread onto the lyophobic matrix and have contact angle θ_δ. For intermediate volumes, one encounters the droplet regime (II) for which the contact angle does not satisfy the Young equation. Instead, it fulfills the inequalities [1]

$$\theta_\gamma \le \theta \le \theta_\delta \quad \text{for regime (II)} \tag{5.1}$$

In this regime, the contact line is pinned to the circular domain boundary and the ($\alpha\beta$) interface

forms a spherical cap. The latter shape is a simple example of a constant mean curvature surface with a prescribed edge. It is important to note that the mean curvature is not monotonic with increasing droplet volume but reaches a maximum value as the droplet attains the shape of a half sphere, i.e. as the contact angle attains the value $\theta = \pi/2$.

For a circular domain boundary, it is intuitively clear that a spherical cap is the state of lowest free energy. In particular, any shape for which the contact line is partially pinned to and partially detached from the circular domain boundary should have a larger free energy. In general, however, this is not true. One counterexample is provided by a channel on a striped (γ) domain which develops a bulge, see Section 5.3 below. If the contact angle θ_γ of the lyophilic stripe is sufficiently small and the stripe is sufficiently long the bulge state of the channel is characterized by a contact line which detaches itself partially from the boundary of the lyophilic (γ) domain and makes an excursion across the lyophobic (δ) matrix.

In general, it is easy to see that the contact line will often detach itself from the domain boundary if the surface domain is not convex (outwards). For example, consider a lyophilic domain which consists of two circular parts connected by a thin stripe. In this case, the contact line will tend to complete one of the circular domain boundaries. This corresponds to the intermediate droplet regime (I/II) in which the contact line runs both across the lyophilic (γ) domain and along the ($\gamma\delta$) domain boundary. Another example is provided by a domain boundary which has an invagination. In this case, the contact line will tend to bridge the invagination and thus to cross the lyophobic (δ) matrix. The latter shape belongs to the intermediate regime (II/III).

It is therefore convenient to consider first the limiting case of strongly lyophilic and strongly lyophobic surface domains with $\theta_\gamma = 0$ and $\theta_\delta = \pi$, respectively. In this limit, the contact line must be pinned to the domain boundary, and the ($\alpha\beta$) interface of the droplet is a constant mean curvature surface attached to this boundary irrespective

of the boundary shape. In addition, it follows from a general nonexistence theorem [32,33] that the mean curvature cannot exceed a certain maximal value. This implies again that the mean curvature exhibits a maximum as a function of the droplet volume. Note that, for a general shape of the domain boundary, the droplet will be non-axisymmetric and, thus, can no longer be characterized by a unique contact angle.

From a mathematical point of view, the generalized Young equation (2.5) corresponds to the transversality condition which arises from the free variation of the contact line. If this variation is constrained and the contact line is pinned, the transversality condition is lost and the contact angle can freely adjust its value within a certain range as in Eq. (5.1). It is interesting to note that an analogous situation occurs for the adhesion of vesicles to solid substrates. In this latter case, the free variation of the contact line leads to a transversality condition for the mean curvature M^* along the contact line as given by [34,35]

$$M^* = (W/2\kappa)^{1/2} \tag{5.2}$$

where W and κ are the adhesion free energy per unit area and the bending rigidity of the vesicle membrane, respectively. If the substrate surface contains (γ) and (δ) domains characterized by adhesive strength W_γ and $W_\delta < W_\gamma$, one must again distinguish several regimes in complete analogy to those discussed for droplets above. Thus, if the contact line of the vesicle is pinned to the $(\gamma\delta)$ domain boundary, the contact mean curvature is no longer fixed but satisfies the inequalities

$$(W_\gamma/2\kappa)^{1/2} > M^* > (W_\delta/2\kappa)^{1/2} \tag{5.3}$$

5.2. Droplet pattern on several surface domains

The experimental procedures used to create structured or imprinted substrate surfaces typically generate whole arrays or patterns consisting of many surface domains. Therefore, let us consider a surface pattern consisting of N identical domains, which are lyophilic with $\theta_\gamma = 0$, on an otherwise lyophobic matrix with $\theta_\delta = \pi$. For simplicity, the domains are taken to be circular in this section. We now place a certain amount of (β) phase onto these circular domains and look for the wetting morphology of lowest free energy.

This statistical ensemble describes three somewhat different physical situations. (i) Fluid–fluid systems at two phase coexistence for which the amount of (β) phase is controlled by the total volume of the system and the total number of particles. (ii) Fluid–fluid systems off coexistence for which the (α) phase in the bulk is slightly supersaturated but still (meta)stable. At the lyophilic surface domains. the nucleation barriers are strongly reduced, however, and the (β) phase starts to condense at those domains. In this case, the amount of liquid increases with time, but if this growth process is slow, the resulting time evolution of the droplet morphology should resemble a sequence of equilibrium states as considered here. (iii) Nonvolatile liquids which are placed onto the structured surface by pipettes or other means. For this latter case, the lowest free energy state corresponds to the most probable droplet morphology. In practice, the droplets in case (iii) will be typically in one of many metastable states which depends on the preparation method and one has to perturb the system externally in order to attain a different morphology of lower free energy.

The droplets on the different surface domains must all have the same mean curvature M because of the Laplace equation $2M\Sigma_{\alpha\beta} = P_\beta - P_\alpha$ as given by Eq. (2.4). For a spherical cap, M is simply the inverse of the radius of the sphere. In addition, the contact area of these droplets is fixed to be identical with the area of the circular surface domains (since we look at the limiting case with $\theta_\gamma = 0$ and $\theta_\delta = \pi$). This implies that the ensemble of droplets can only consist of two different types of droplets: small ones with contact angle θ_{sm} and large ones with contact angle θ_{la}. If one combines a small droplet with a large one in such a way that they are pasted together along their flat contact areas, one obtains a complete sphere which implies $\theta_{sm} + \theta_{la} = \pi$.

One must now consider different arrangements consisting of N_{sm} small and N_{la} large droplets with

(A)

(B)

(C)

(D)
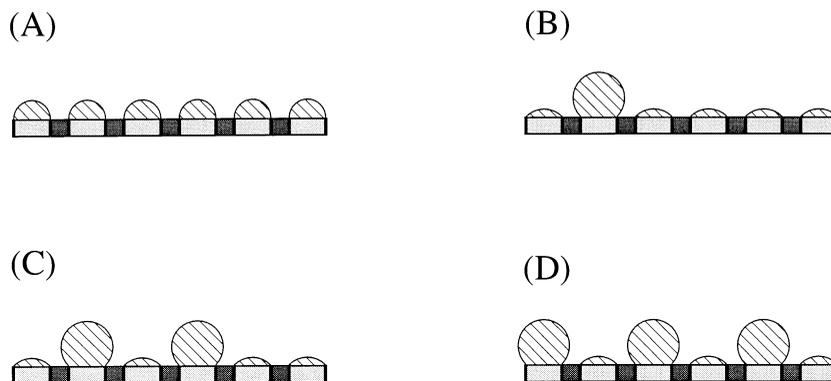
Fig. 3. Possible droplet patterns on a lattice of circular domains. In each configuration, all droplets must have the same mean curvature which implies that the small and the large droplet form a complete sphere when pasted together along their flat contact area. Droplet patterns such as (C) and (D) that contain more than one large droplet are unstable and must decay either into the homogeneous pattern (A) or into the inhomogeneous pattern (B) with only one large droplet.

$N_{sm} + N_{la} = N$ as shown in Fig. 3. Somewhat surprisingly, a systematic calculation of the corresponding free energies [1] shows that only two of these possible arrangements represent stable or metastable states: (i) the homogeneous droplet pattern, denoted by (A), consisting of an array of identical droplets see Fig. 3(A); and (ii) heterogeneous droplet patterns denoted by (B) consisting of only one large droplet and $N-1$ small ones as shown in Fig. 3(B). This pattern is N-fold degenerate since the large droplet can sit on any of the N domains. All other droplet patterns which contain two or more large droplets are saddle points in shape space and must decay into the patterns (A) or (B).

Thus, for N identical surface domains, the wetting phase can exhibit two (meta)stable droplet patterns. If one has a large lattice of surface domains (as can be easily prepared experimentally), one should also consider a third morphology given by a film state which buries all lyophilic surface domains. Such a state can be realized by appropriate boundary conditions; for instance, one may add confining walls of phase (ε) perpendicular to the structured surface with contact angle $\theta_\varepsilon \simeq \pi/2$. Under such circumstances, a film state, denoted by (F), will be the most favorable for the (β) phase as soon as its volume exceeds a critical value.

In summary, the wetting phase can exhibit three different types of morphologies as shown in Fig. 4: (i) a homogeneous droplet pattern (A) where all droplets are identical and, thus, have the same shape and contact angle; (ii) a heterogeneous droplet pattern (B) characterized by one large and many small droplets; and (iii) a film state (F) for which the wetting phase covers both the lyophilic and the lyophobic surface regions.

The relevant parameters which determine the shape phase diagram in Fig. 4 are: (i) the liquid volume V/N per lyophilic domain; and (ii) the area fraction ϕ_γ of the lyophilic domains. As one
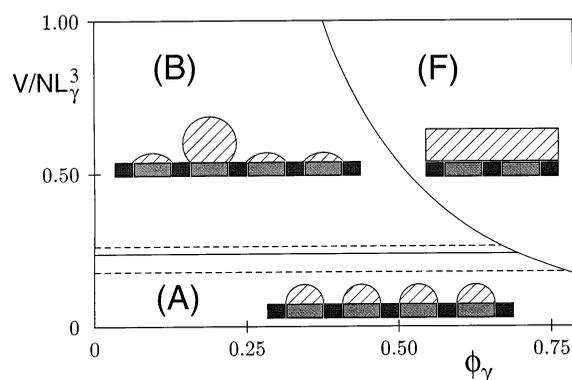
Fig. 4. Morphological phase diagram for droplets on N circular domains with diameter L_γ as determined by the reduced volume V/NL_γ^3 and the area fraction ϕ_γ of the lyophilic domains. The numerical values correspond to the case $N = 4$.
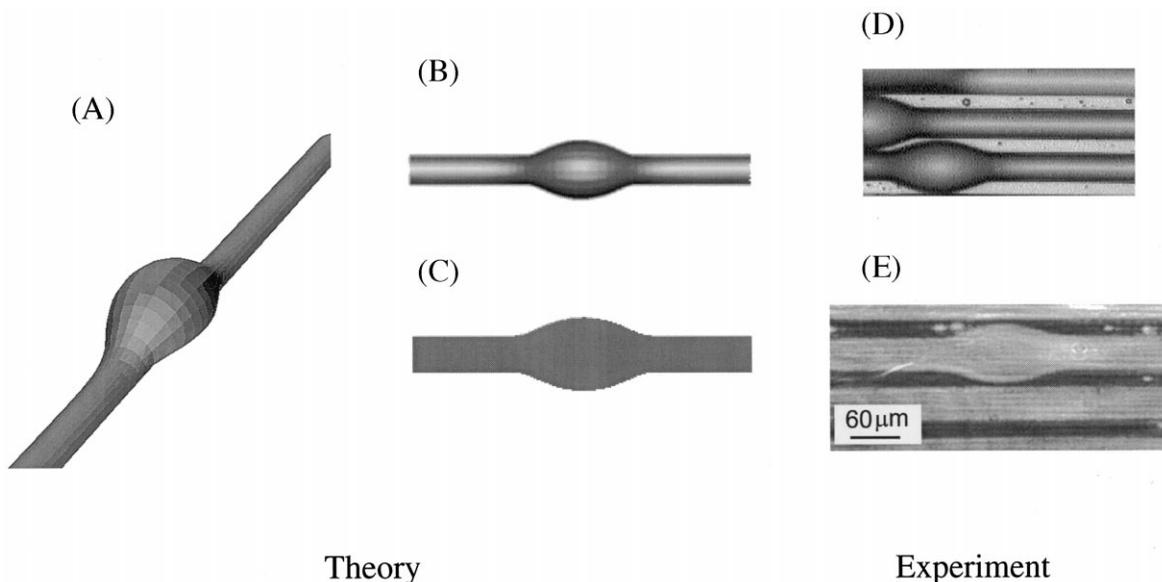
Fig. 5. (A) Bulge state of microchannel as determined theoretically: (B,D) projection of the shape perpendicular to the substrate; and (C,E) location of the contact line which makes an excursion into the hydrophobic surface domains. (B,C) are obtained from the theoretical shape, (D,E) from the experimental observations.

moves across the phase boundaries, the wetting phase undergoes transitions between these different morphologies.

The transition from the homogeneous to the heterogeneous droplet pattern is continuous for $N = 2$ but discontinuous for $N > 2$. For $N = 2$, the critical contact angle $\theta_{AB}^*(N = 2) = \pi/2$. For $N > 2$, one has a hysteresis loop for the contact angle range $\theta_{AB}^{\min}(N) < \theta < \theta_{AB}^{\max}(N)$ where $\theta_{AB}^{\max}(N)$ has the universal value [1]

$$\theta_{AB}^{\max}(N) = \pi/2 \quad \text{for all } N \qquad (5.4)$$

This latter value is intimately related to the non-monotonic behavior of the mean curvature for the single domain case. As mentioned in the previous section, the mean curvature of the droplet as a function of the contact angle θ has a maximum at $\theta = \pi/2$. The latter value corresponds to the volume of a half sphere. Since such a nonmonotonic behavior of the mean curvature as a function of the droplet volume applies to domains of arbitrary shape, the morphological transition from the homogeneous (A) to the heterogeneous (B) state should be present for N domains with identical but arbitrary shape.

5.3. Channels on striped surfaces

The transition from the homogeneous pattern (A) to the heterogeneous pattern (B) as discussed in the previous subsection has interesting consequences for the shape of a liquid channel on a striped surface domain. Thus, consider a lyophilic stripe on a lyophobic surface. If one deposits a small amount of liquid on this stripe, one obtains a channel which is homogeneous and has the shape of a cylinder segment with constant cross-section. As the volume of this channel is increased, the channel grows until it undergoes a sudden transition to a morphologically different channel state which now exhibits a single bulge, see Fig. 5. [3]

The channel instability and the bulge state were observed experimentally using: (i) optical microscopy to obtain the contours of the liquid surface when projected perpendicular to the substrate, see Fig. 5(D); and (ii) evanescent wave microscopy to measure the position of the contact lines of the channel along the substrate, see Fig. 5(E). In this example, the contact angle for the lyophilic and the lyophobic surface domains was $\theta_\gamma \simeq \pi/36$ and $\theta_\gamma \simeq 3\pi/5$, respectively.

Using these values for the contact angles, we calculated the full three-dimensional shape of the channel as shown in Fig. 5(A) from which we determined its projected shape displayed in Fig. 5(B) and the position of the contact line as in Fig. 5(C). Direct inspection of Fig. 5 shows that the experimental and the theoretical shapes are in good agreement. As explained, the theoretical shapes have been calculated from a model which does not include line tension terms. This implies that the crossover scale L_β^* must lie below a couple of micrometers and that the line tension Λ must be below 10^{-7} J m^{-1}.

The channel instability is rather different from the classical Rayleigh–Plateau instability [36], which is characterized by the decay of a free standing cylinder into a periodic array of many droplets. In contrast, the morphological transition discussed here leads to a single bulge of the channel. Furthermore, while the free standing cylinder will always undergo a Rayleigh–Plateau instability, the homogeneous channel turns out to be stable as long as its volume is sufficiently small.

Some insight into the morphological transition of the channel can be obtained from a stability analysis of its homogeneous state with constant cross section and constant contact angle θ. In order to determine the stability of this state, one must then study shape deformations of these cylinder segments which (i) conserve the liquid volume and (ii) leave the position of the contact line unchanged. From this linear stability analysis, one finds that the cylinder is locally stable for contact angle $\theta < \pi/2$ but unstable for $\theta > \pi/2$ provided the wavelength L of the shape deformation exceeds a certain threshold value L_c. This threshold value is given by [3]

$$L_c = \left[\frac{\pi/2}{\theta^2 - (\pi/2)^2} \right]^{1/2} \frac{\theta}{\sin(\theta)} L_\gamma \qquad (5.5)$$

which depends on θ and on the width L_γ of the lyophilic stripe.

Thus, we conclude that the cylindrical channel is unstable if the contact angle becomes larger than $\pi/2$. It is important to note, however, that the linear stability analysis cannot give us information about the new state into which the homogeneous channel decays. Further insight into this new state

can be obtained by comparison with the droplet patterns discussed in the previous subsection.

Indeed, all we have to do is to replace the lyophilic stripe by a linear array of N circular domains. As discussed in the previous subsection, such an array leads to a morphological transition between a homogeneous droplet pattern (A) and an inhomogeneous droplet pattern (B) with one large droplet. Thus, we find a rather close analogy (i) between the homogeneous channel and the homogeneous droplet pattern (A) and (ii) between the bulging channel and the heterogeneous droplet pattern (B) with one large droplet. We see that the channel instability is intimately related to the transition from (A) to (B).

The bifurcation structure underlying the channel instability implies that this morphological transition is rather universal. Indeed, our calculations show that it applies to any liquid on any striped surface provided that the contact angle on the lyophilic stripes is sufficiently small and the stripe is sufficiently long. Indeed, the same transition can be studied for tin channels on metallic surface stripes as used for soldering. [37] Thus, the channel instability must have been observed many times in commonly used soldering processes but it has not been realized that this instability represents a morphological wetting transition.

6. Line tension effects

In the previous sections, we neglected line tension effects since the size of the surface domains and the characteristic size L_β of the wetting structures were taken to be large compared to the crossover scale $L_\beta^* \simeq |\Lambda|/\Sigma_{\alpha\beta}$. Now, let us consider smaller domain sizes and wetting structures for which the line tension should have an observable effect on the droplet morphologies.

As before, the substrate surface is again taken to consist of two types of surface domains, either lyophilic (γ) or lyophobic (δ). In addition to the position-dependent interfacial tension as given by Eq. (4.4), one should now consider a position dependent line tension $\Lambda = \Lambda(\mathbf{x})$ which is also taken to be piece-wise constant and which can attain three different values:

$$\Lambda(\mathbf{x}) = \Lambda_\gamma \quad \text{for } \mathbf{x} \text{ within the } (\gamma) \text{ domain}$$
$$= \Lambda_\delta \quad \text{for } \mathbf{x} \text{ within the } (\delta) \text{ domain}$$
$$= \Lambda_{\gamma\delta} \quad \text{for } \mathbf{x} \text{ at the } (\gamma\delta) \text{ domain boundary}$$
$$(6.1)$$

At this point, it is useful to recall that the line tension enters the generalized Young equation (2.6) only in the form of a two-dimensional divergence as given by $\nabla_x \cdot (\Lambda(\mathbf{x})\hat{n})$ where the vector $\hat{n}$ is normal to the contact line see Appendix A.2. This implies that the product $\Lambda\hat{n}$ has to be continuous along the contact line.

For $\Lambda_\gamma \simeq \Lambda_\delta \simeq \Lambda_{\gamma\delta}$, one recovers the case of a uniform line tension $\Lambda = $ constant. If this latter line tension is positive, it will act to decrease (i) the length of the contact line and (ii) the contact area of the droplet with the substrate surface. For a homogeneous substrate, these effects have been recently discussed in Ref. [38]. On the other hand, for a surface with extended surface domains which are comparable to or smaller than $L_\beta^* \simeq |\Lambda|/\Sigma_{\alpha\beta}$, the line tension will change the 'phase' boundaries between the different droplet regimes (I)–(III) introduced in Section 5.1. Thus, the contact line will try to make 'shortcuts' in order to decrease its length even if this leads to an increase in the area of the $(\alpha\beta)$ interface.

Note that a constant value of the line tension Λ together with the previously mentioned continuity of the product $\Lambda\hat{n}$ implies that the normal vector varies smoothly along the contact line. Therefore, the latter line has no kinks if the line tension is uniform. This changes, however, as soon as we consider the general case in which the three values of $\Lambda(\mathbf{x})$ as given by Eq. (6.1) have to be distinguished. In this latter situation, the continuity of $\Lambda\hat{n}$ together with the piece-wise constant variation of Λ implies that the normal vector $\hat{n}$ jumps if the contact line moves across the $(\gamma\delta)$ domain boundary. Therefore, the contact line exhibits a kink as soon as it hits such a boundary.

7. Summary and outlook

In summary, we have discussed a general theoretical framework for wetting and dewetting on structured and imprinted surfaces. This framework leads to new types of wetting transitions at which the wetting phase changes its morphology. As explained in Section 3, this framework is based on an appropriate separation of length scales. As the surface domains and the wetting structures become smaller and smaller, more and more length scales have to be taken into account in order to determine the wetting morphology. We have identified several such scales for the spatial extension of the contact line (Section 3.2 and Section 3.3), in the context of the Cassie equation (Section 4.2), and for interfacial folds emanating from the contact line (Section 4.3).

On sufficiently large scales beyond the crossover length $L_\beta^* \simeq |\Lambda|/\Sigma_{\alpha\beta}$ introduced in Eq. (3.11), the line tension terms are irrelevant and the wetting morphologies are governed by the interfacial tensions as discussed in Sections 4 and 5. In Section 5.3, we have described the detailed comparison between experimentally observed and theoretically determined shapes [3] which shows explicitly that line tension effects can be ignored in the systems under consideration.

In the last Section 6, our description was extended in order to include such line tension effects. If the line tension is uniform, the contact line should vary smoothly and exhibit no kinks. However, if the line tension at the lyophilic domains differs significantly from the line tension at the lyophobic domains, the contact line should exhibit a kink at the domain boundary.

The work described here has been extended to several related but distinct geometries: (i) channels on ring shaped surface domains — in this case, a nonuniform channel state with a single bulge is found which is degenerate since it can be anywhere along the ring domain [39]; (ii) perforated wetting layers on a lattice of lyophobic domains — in the latter case, one has a morphological transition between a perforated layer and a layer of uniform thickness [15]; and (iii) a slab geometry bounded by two structured surfaces — this leads to the formation of liquid bridges and, thus, to effective forces between these two surfaces [40].

All of these systems are accessible to experiments. Thus, these systems provide new opportunities for fruitful interaction between theory and experiment.

Appendix A

Geometry of the wetting layer

The wetting layer of (β) phase occupies the spatial region $\mathscr{V}$. This region may consist of several disconnected components; one example is a wetting layer which consists of several droplets. The spatial region occupied by the (β) phase is bounded by its interfaces with the fluid (α) phase and the solid (σ) substrate. In general, even a simply connected region $\mathscr{V}$ can be bounded by several disconnected $(\alpha\beta)$ interfaces; one example is a droplet which covers a bubble of (α) phase. Likewise, the (β) phase may form an arch between two disconnected domains of the substrate surface corresponding to two disjoint $(\beta\sigma)$ interfaces.

The total surface region of the $(\alpha\beta)$ interfaces and of the $(\beta\sigma)$ interfaces will be denoted by $\mathscr{A}_{\alpha\beta}$ and $\mathscr{A}_{\beta\sigma}$, respectively. The surface region $\mathscr{A}_{\beta\sigma}$ represents the contact region between the wetting layer and the substrate. The two types of interfaces meet along the $(\alpha\beta\sigma)$ contact line(s) $\mathscr{L} \equiv \mathscr{L}_{\alpha\beta\sigma}$.

The total volume of the wetting phase is $V \equiv |\mathscr{V}|$ where the notation $|\mathscr{S}|$ is used for the content (i.e. length or area or volume) of the set $\mathscr{S}$. The total surface area of the $(\alpha\beta)$ interfaces and of the $(\beta\sigma)$ interfaces is given by $A_{\alpha\beta} \equiv |\mathscr{A}_{\alpha\beta}|$ and the contact area $A_{\beta\sigma} \equiv |\mathscr{A}_{\beta\sigma}|$, respectively. The total length of the contact line(s) is $L \equiv |\mathscr{L}|$.

We consider (σ) substrates which are relatively rigid and assume that the shape of the substrate surface remains essentially unchanged during the wetting process. The $(\beta\sigma)$ interface is taken to lie within the substrate surface, i.e. we ignore any intrinsic small scale structure of this interface. In the present paper, we also assume that the topography or roughness of the substrate surface is small compared to the lateral size of the surface domains. Thus, we focus on the simplest possible geometry which is that given by a planar substrate surface. The Cartesian coordinate parallel to this plane and, thus, to the $(\beta\sigma)$ interface is denoted by $\mathbf{x} \equiv (x_1, x_2)$.

In contrast to the $(\beta\sigma)$ interface, the $(\alpha\beta)$ interface between the two fluid phases can be easily deformed. Thus, we will parametrize the surface of this interface in a general way as described in the next subsection.

Appendix A.1

Parametrization of $(\alpha\beta)$ interface

The shape of the $(\alpha\beta)$ interface is parametrized by $\vec{R}(\mathbf{S})$ with the internal surface coordinate $\mathbf{S} \equiv (S^1, S^2)$ (we use the convention that a three-dimensional vector is indicated by an arrow while a two-dimensional vector is written in boldface). At each point on the $(\alpha\beta)$ interface, there are two tangent vectors $\partial_i \vec{R} \equiv \partial \vec{R}/\partial S^i$ with $i = 1, 2$. The orientation of the two surface coordinates is chosen in such a way that the normal vector $\hat{N} \equiv (\partial_1 \vec{R} \times \partial_2 \vec{R})/|\partial_1 \vec{R} \times \partial_2 \vec{R}|$, points away from or out of the wetting layer.

It is sometimes useful to consider the total surface surrounding the wetting layer which consists of all $(\alpha\beta)$ and $(\beta\sigma)$ interfaces. All normal vectors of this surface are then taken to point away from the (β) phase. This implies that the normal vectors of the $(\beta\sigma)$ interface point into the substrate.

All properties related to the intrinsic geometry of the $(\alpha\beta)$ interface are expressed in terms of the metric tensor defined by

$$g_{ij} \equiv \partial_i \vec{R} \cdot \partial_j \vec{R} \qquad (A.1)$$

Two important quantities are the determinant and the inverse of the metric given by

$$g_{ij} \equiv \det(g_{ij}) \quad \text{and} \quad g^{ij} \equiv (g_{ij})^{-1} \qquad (A.2)$$

In addition, one has to consider the (extrinsic) curvature tensor defined by

$$h_{ij} = \hat{N} \cdot \partial_i \partial_j \vec{R} = -\partial_i \hat{N} \cdot \partial_j \vec{R} \qquad (A.3)$$

The mean curvature M and the Gaußian curvature G are now obtained via

$$M \equiv -\frac{1}{2}\,\mathrm{tr}(h_{ik}g^{kj}) \ \ \text{and} \ \ G \equiv \det(h_{ik}g^{kj}) \qquad (A.4)$$

where repeated indices are implicitly summed over. Note that the definition of M contains a minus sign which ensures that the mean curvature M of a spherical cap with radius R_o is positive and given by $M = +1/R_o$.

Appendix A.2

Parametrization of the contact line

For simplicity, let us now focus on a single droplet, i.e. on a wetting layer which is bounded by a simply connected $(\alpha\beta)$ interface with a single contact line $\mathscr{L}$. This contact line is parametrized by $\vec{r}(s)$ with arclength s. Its tangent vector $\hat{t} \equiv d\vec{r}(s)/ds$ has unit length, see Fig. 6.

For general space curves, one defines two normal vectors, the principal normal and the binormal. In the present context, it is more convenient to use the normal vector $\hat{n}$ with the following two properties: (i) it lies in the plane tangential to the substrate surface; and (ii) it has the same orientation as the normal vectors $\hat{N}$ of the $(\alpha\beta)$ interface.

If the substrate surface had an arbitrary shape, the plane tangential to this surface would not be identical, in general, with the osculating plane of the contact line, and the normal vector $\hat{n}$ would not be equal to the principal normal. For a planar substrate surface, however, the two planes coincide and $\hat{n}$ does represent the principal normal of the contact line.

We also require that the unit vectors $\hat{t}$ and $\hat{n}$ have the same right-handed orientation as $\hat{x}_1$ and $\hat{x}_2$. This implies that one has chosen a clockwise direction of the contact line (when viewed from the half space with positive z), see Fig. 6.

The curvature $C_{\alpha\beta\sigma}$ of the contact line is defined by

$$C_{\alpha\beta\sigma} \equiv -\hat{n} \cdot \frac{d^2\vec{r}}{ds^2} = -\hat{n} \cdot \frac{d\hat{t}}{ds} \qquad (A.5)$$

As with the mean curvature M, a minus sign has been included in the definition of $C_{\alpha\beta\sigma}$ in order to ensure that $C_{\alpha\beta\sigma} = +1/R_{\parallel}$ for a planar circle of radius $R_{\parallel}$.

Appendix A.3

Geometric relation between mean curvature and contact angles

We still consider a single droplet as in the previous subsection. In equilibrium, the mean curvature M of such a droplet is constant and is determined by the Laplace equation (2.4). In addition, one has a simple geometric relation between M and the local contact angles $\theta = \theta(s)$ of the droplet along its contact line as is shown in the following.

First, the mean curvature M can be expressed as

$$2M = -\nabla_x \cdot \hat{N}_{\parallel} \qquad (A.6)$$

where ∇_x represents the two-dimensional gradient and $\hat{N}_{\parallel}$ is the projection of the interfacial normal vector $\hat{N}$ onto the **x**-plane.

Now, let us integrate Eq. (A.6) over a bounded region Ω within the **x**-plane. The boundary $\partial\Omega$ has length $L_b \equiv |\partial\Omega|$ and can be parametrized by its arclength s. It then follows from the divergence theorems that the surface integral over Ω can be transformed according to

$$\int_{\Omega} dx_1 dx_2 \nabla_x \cdot \vec{v}_{\parallel} = -\int_0^{L_b} ds\, \hat{n} \cdot \vec{v}_{\parallel} \qquad (A.7)$$
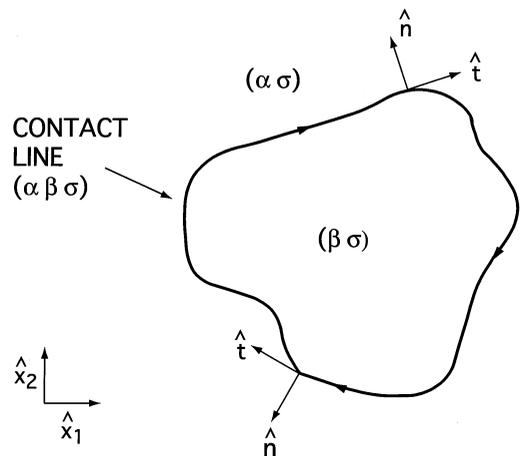
Fig. 6. The contact line is parametrized by its arclength and has tangential vector $\hat{t}$ and normal vector $\hat{n}$ which both lie within the **x**-plane of the substrate surface with $\mathbf{x} = (x_1, x_2)$. The unit vectors t and n have the same orientation as the unit vectors $\hat{x}_1$ and $\hat{x}_2$.

for any projected vector field $\vec{v}_{\parallel}$, where $\hat{n}$ is the normal vector defined in Fig. 6. If we use this identity with $\vec{v}_{\parallel} = \hat{N}_{\parallel}$, the surface integral over the mean curvature is transformed into a line integral over $\hat{n} \cdot \hat{N}_{\parallel}$.

For a planar substrate surface (parallel to the **x**-plane), one also has

$$\hat{n} \cdot \hat{N}_{\parallel} = (\hat{n}, 0) \cdot \hat{N} = \sin(\theta(s)) \qquad (A.8)$$

along the contact line where $\theta(s)$ is the local contact angle. If this expression is inserted into (A.7) with $\vec{v}_{\parallel} = \hat{N}_{\parallel}$ and the surface integral is extended to cover the contact region $\mathscr{A}_{\beta\sigma}$, one arrives at

$$2MA_{\beta\sigma} = \int_0^L ds\, \sin(\theta(s)) \equiv L\langle \sin(\theta)\rangle \qquad (A.9)$$

where $A_{\beta\sigma}$ and L are again the contact area and the length of the contact line, respectively, and we have used the fact that the mean curvature M of the droplet is constant. Note that this relation between the mean curvature M and the contact angles θ does not depend on the line tension Λ.

Appendix B

List of mathematical symbols

All symbols are ordered alphabetically. Small letters precede capital letters. Symbols with subscripts are treated as combined words.

A surface or interfacial area, $A \equiv |\mathscr{A}|$
$\mathscr{A}$ surface region
α vapor phase (in general, fluid phase)
β liquid phase which forms the wetting layer
$C_{\alpha\beta\sigma}$ curvature of the contact line
δ lyophobic substrate
ΔP pressure difference, $\Delta P \equiv P_\alpha - P_\beta$
$\mathscr{F}$ free energy
g gravitational acceleration
γ lyophilic substrate
κ bending rigidity of membrane
l local thickness of wetting layer
l_{min} local thickness at which effective interface potential has a minimum

l_{pin} thickness at which effective interface potential has a point of inflection
ℓ microscopic length scale
ℓ_{mol} size of molecules
ℓ_{pot} potential range of substrate potential
$\ell_{\sigma\parallel}$ length scale for composition fluctuations in the substrate
$\ell_{\sigma\perp}$ length scale for topographical roughness of the substrate
L mesoscopic or macroscopic length scale
L_β linear dimension of wetting structure of (β) phase
$L_{\alpha\beta\sigma}$ length of contact line(s), $L_{\alpha\beta\sigma} \equiv |\mathscr{L}_{\alpha\beta\sigma}|$
L_{cap} capillary length
$\mathscr{L}_{\alpha\beta\sigma}$ contact line(s)
Λ line tension of contact line, $\Lambda \equiv \Lambda_{\alpha\beta\sigma}$
M mean curvature of the interface or surface
$\hat{n}$ unit vector which is normal to contact line (within the plane tangential to the substrate)
N number of surface domains
$\hat{N}$ unit vector which is normal to interface
N_α particle number density of (α) phase
$N_{\alpha\beta}$ particle number density at ($\alpha\beta$) interface
P Pressure
ϕ surface composition of the (σ) substrate as measured by the area fraction
ϕ_γ area fraction of lyophilic surface domains
T temperature (in energy units)
$\vec{r}$ position of contact line, $\vec{r} = \vec{r}(s)$
$\vec{R}$ position of ($\alpha\beta$) interface, $\vec{R} = \vec{R}(\mathbf{S})$
s arclength parameter of contact line
$\mathbf{S}$ intrinsic coordinate for ($\alpha\beta$) interface, $\mathbf{S} \equiv (S^1, S^2)$
σ substrate or solid phase
$\Sigma_{\alpha\beta}$ surface tension of ($\alpha\beta$) interface
$\hat{t}$ unit tangent vector to contact line, $\hat{t} \equiv d\vec{r}(s)/ds$
θ contact angle
θ_∞ contact angle of large droplets on a flat and homogeneous substrate
U effective interface potential
V volume, $V \equiv |\mathscr{V}|$
$\mathscr{V}$ spatial region
W adhesive strength = adhesion free energy per unit area

x	Cartesian coordinate parallel to substrate, $\mathbf{x} \equiv (x_1, x_2)$
$\xi_{\alpha\beta}$	interfacial correlation length
z	Cartesian coordinate perpendicular to substrate

References

[1] P. Lenz, R. Lipowsky, Phys. Rev. Lett. 80 (1920) 1998.

[2] P.S. Swain, R. Lipowsky, Langmuir 14 (1998) 6772.

[3] H. Gau, S. Herminghaus, P. Lenz, R. Lipowsky, Science 283 (1999) 46.

[4] G. Lopez, H. Biebuyck, C. Frisbie, G.M. Whitesides, Science 260 (1993) 647.

[5] J. Drelich, J.D. Miller, A. Kumar, G.M. Whitesides, Colloids Surf. A 93 (1994) 1.

[6] F. Morhard, J. Schumacher, A. Lenenbach, T. Wilhelm, R. Dahint, M. Grunze, D.S. Everhart, Electrochem. Soc. Proc. 97 (1997) 1058.

[7] K. Jacobs, H. Gau, S. Schlagowski, W. Mönch, T. Pompe, A. Fery, S. Herminghaus, in: Proceedings of the 2nd European Coating Symposium, Strasbourg, 1997 (to be published).

[8] G. Möller, M. Harke, H. Motschmann, Langmuir 14 (1998) 4955.

[9] F. Burmeister, C. Schäfle, T. Matthes, M. Bohmisch, J. Boneberg, P. Leiderer, Langmuir 13 (1997) 2983.

[10] U. Drodofsky, J. Stuhler, T. Schulze, M. Drewsen, B. Brezger, T. Pfau, J. Mlynek, Appl. Phys. B 65 (1997) 755.

[11] J. Heier, E.J. Kramer, S. Walheim, G. Krausch, Macromolecules 30 (1997) 6610.

[12] R. Lipowsky, Critical Behavior of Interfaces: Wetting, Surface Melting and Related Phenomena, Jül-Spez-438 (ISSN 0343-7639), Forschungszentrum (KFA), Jülich, 1987.

[13] J. Rowlinson, B. Widom, Molecular Theory of Capillarity, Clarendon Press, Oxford, 1982.

[14] D. Li, Colloids Surf. A 116 (1996) 1.

[15] P. Lenz, Benetzungsphänomene auf strukturierten Substraten, doctoral thesis, Universität Potsdam, 1998.

[16] P. Lenz, R. Lipowsky, Stability of droplets on homogeneous and structured surfaces, in preparation.

[17] L. BoruvLa, A.W. Neumann, J. Chem. Phys. 66 (1977) 5464.

[18] A.I. Rusanov, Colloid J. USSR Engl. Transl. 39 (1977) 618.

[19] A. Marmur, Colloids and Surf. A Physiochem. Eng. Aspects 136 (1998) 81.

[20] J. Gaydos, A.W. Neumann, in: A.W. Neumann, J.K. Spelt (Eds.), Applied Surface Thermodynamics, Marcel Dekker, New York, 1996, pp. 169–238.

[21] J. Drelich, Colloids Surf. A 116 (1996) 43.

[22] T. Pompe, A. Fery, S. Herminghaus, Langmuir 14 (1998) 2585.

[23] R. Lipowsky, D. Kroll, R.K.P. Zia, Phys. Rev. B 27 (1983) 4499.

[24] E. Brézin, B. Halperin, S. Leibler, J. Physique 44 (1983) 775.

[25] R. Lipowsky, Phys. Rev. Lett. 52 (1984) 1429.

[26] R. Lipowsky, Phys. Rev. B 32 (1985) 1731.

[27] R. Lipowsky, M.E. Fisher, Phys. Rev. B 36 (1987) 2126.

[28] M.W. Cole, E. Vittoratos, J. Low Temp. Phys. 22 (1976) 223.

[29] W. Koch, S. Dietrich, M. Napiorkowski, Phys. Rev. E 51 (1995) 3300.

[30] M. Schön, D.J. Diestler, Chem. Phys. Lett. 270 (1997) 339.

[31] A. Cassie, Discuss. Faraday Soc. 3 (1948) 11.

[32] M. Struwe, Plateau's Problem and the Calculus of Variations, Princeton University Press, Princeton, NJ, 1988.

[33] J. Sullivan, F. Morgan, Int. J. Math. 7 (1996) 833.

[34] U. Seifert, R. Lipowsky, Phys. Rev. A 42 (1990) 4768.

[35] R. Lipowsky, U. Seifert, Mol. Cryst. Liq. Cryst. 202 (1991) 17.

[36] S. Chandrasekhar, Hydrodynamic and Hydromagnetic Stability, Dover, New York, 1981.

[37] W. Fenzl, P. Lenz, R. Lipowsky, Morphological transitions of soldering channels, in preparation.

[38] B. Widom, J. Phys. Chem. 99 (1995) 2803.

[39] P. Lenz, R. Lipowsky, Wetting of ring-shaped surface domains, in preparation.

[40] P.S. Swain, R. Lipowsky, Wetting between structured surfaces, preprint.